THE JOURNAL OF PHYSICAL CHEMISTRY B

Article

pubs.acs.org/JPCB

Interparticle Dispersion, Membrane Curvature, and Penetration Induced by Single-Walled Carbon Nanotubes Wrapped with Lipids and PEGylated Lipids

Hwankyu Lee*

Department of Chemical Engineering, Dankook University, Yongin, 448-701, South Korea

ABSTRACT: Single-walled carbon nanotubes (SWNTs) wrapped with different types of lipids and polyethylene glycol (PEG)-grafted lipids were simulated with lipid bilayers. Simulations were carried out with the previously parametrized coarse-grained (CG) SWNT and PEG force fields that had captured the experimentally observed conformations of self-assembled SWNT–lipid complexes and phase behavior of PEG-grafted lipids. Simulations of multiple copies of the SWNT in water show that all pure SWNTs aggregate, lipid-wrapped SWNTs partially aggregate, but those wrapped with lipids grafted to PEG (M_w = 550) completely disperse, indicating the effect of short PEG chains on interparticle aggregation, in agreement with experiment. Starting with initial SWNT orientation parallel to the bilayer surface, SWNTs wrapped with lysophospholipids and PEG (M_w = 550)-grafted lipids insert into the hydrophobic region of the bilayer, while SWNTs wrapped with phospholipids and longer PEG (M_w = 2000)-grafted lipids do not. These indicate that SWNTs insert because of the hydrophobic interaction with the bilayer tails, but the tight wrapping of charged lipid headgroups and long hydrophilic PEG chains can weaken the hydrophobic interaction and inhibit SWNT insertion. The inserted SWNTs contact the entire tails of neighboring lipids in one leaflet of the bilayer, which disorders the lipid bilayer and induces positive curvature. Our findings indicate that interparticle aggregation, SWNT penetration, and membrane curvature can be modulated by the SWNT–lipid structure and the PEG length.

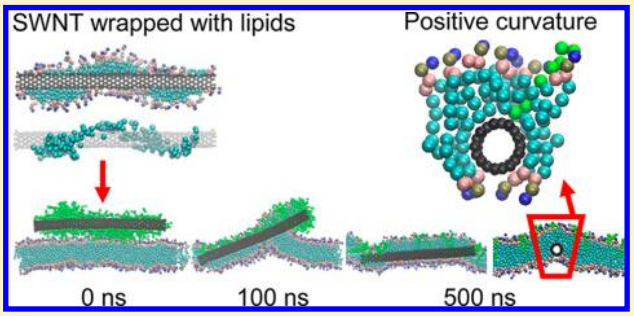

INTRODUCTION

Due to excellent mechanical strength and chemical stability, single-walled carbon nanotubes (SWNTs) have shown great potential for biomedical applications, such as antitumor therapeutics, and gene or drug delivery.[1−8] Interesting ligands, such as drugs, imaging and targeting molecules, can be covalently or noncovalently conjugated to the SWNT and delivered to specific cancer cells.[9,10] These applications require the interaction of the SWNT–ligand complex with cell membranes, which has motivated many experimental studies.[11] To increase solubility, reduce cytotoxicity, and inhibit their aggregation in water, the SWNT surface is often modified by noncovalent wrapping with amphiphiles such as lipids, surfactants, proteins, and soluble polymers.[12−17] The structure and morphology of SWNTs wrapped with different types of lipids were experimentally observed (or proposed) by Ke and co-workers,[18] and were supported by our previous simulations.[19] They performed fluorescence microscopy experiments with cells, which showed translocation and disassembly of the SWNT–lipid complexes through cancer cells, leading to successful gene delivery.[20,21] Dai et al. also showed the effects of the complex structure and conjugation methodologies on cytotoxicity and delivery efficiency.[22−27] Recently, Das et al. found that wrapping of SWNTs with lysophospholipids with a short polyethylene glycol (PEG; M_w = 550) grafted to their headgroups, a process called PEGylation, can significantly inhibit interparticle aggregation.[28] Liu et al. measured the blood circulating lifetime and the organ uptake ratios of SWNTs functionalized with different lengths and conjugate densities of PEG, and optimized the PEG length and density to keep the high circulating lifetime and uptake ratios with the low extent of the SWNT accumulation in skin.[29] While these experiments have provided vital information on the interaction between the modified SWNTs and membranes, results from these are not always easy to interpret at the level of individual molecules, which need to be studied at nearly the atomic scale, as can be done using molecular dynamics (MD) simulations.

MD simulations have been able to explore the SWNT properties and their interactions with lipid bilayers. The Klein group performed coarse-grained (CG) MD simulations of a nanotube with lipid bilayer, showing that SWNTs bind to the bilayer surface and insert into the hydrophobic region of the bilayer.[30] They also analyzed the ordering and flip-flop of lipids around SWNTs, suggesting the penetration mechanism.[31,32] Other CG, dissipative particle dynamics, and constrained all-atom MD simulations showed the effects of the SWNT chirality and size, and the conjugate's properties on the conformation and mechanism of the SWNT penetration.[33−40] Pogodin and

Received: September 7, 2012
Revised: December 4, 2012
Published: December 6, 2012

Baulin calculated the energy required for the SWNT insertion using single-chain mean field theory, which showed that energy higher than that of thermal motion is required for the translocation mechanism.[41] Recently, Ramseyer and co-workers calculated free energies of SWNTs interacting with lipid bilayers from long unconstrained all-atom simulations, showing that the extent of modification of the SWNT surface does not significantly influence the diffusion mechanism of SWNTs into lipid bilayers.[42] These simulations have provided atomic-scale insights into the SWNT−bilayer interaction, but the effects of the structure of SWNTs wrapped with various lipids and PEGs on interparticle aggregation, the SWNT insertion into the bilayer, and the mechanism of the SWNT-induced membrane curvature are still not understood.

In this work, we therefore perform CG MD simulations of SWNTs self-assembled with different types of lipids and PEGylated lipids, which have conformations of "random adsorption", "hemimicelle", "cylindrical micelle", and helical wrapping of "half-cylinder", interacting with lipid bilayers. We first simulate aggregation of three SWNT−lipid complexes in water, showing the effects of the SWNT modification with different lipids and PEGs on interparticle aggregation and diffusivity. Second, a single SWNT−lipid complex is simulated with a lipid bilayer, which reveals the effects of the SWNT−lipid structure and PEGylation on the binding and insertion of SWNTs into the bilayer. The inserted SWNTs disorder the bilayer tails and induce positive curvature, which are rationalized by analyzing the interactions between the SWNT and neighboring lipids.

METHODS

All simulations and analyses were performed using the GROMACS4.5.5 simulation package.[43−45] The "MARTINI" CG force field (FF) was used, which lumps three or four heavy atoms into each CG bead.[46,47] Within the framework of the MARTINI FF, we previously parametrized Lennard-Jones (LJ), electrostatics, bond, angle, and torsional terms of the PEG CG model that predicts densities, conformations, and hydrodynamics, all of which are close to those from all-atom simulations and experiments.[48,49] Our previous simulations with this PEG CG FF successfully captured the phase behaviors of self-assembled liposomes, bicelles, and micelles at the expected ratios of lipids and PEGylated lipids, in agreement with experiment.[50] We also parametrized the SWNT CG model that represents the experimentally observed (or proposed) structures of the self-assembled SWNT−lipid complex, showing the effects of lipid types and PEGylation.[19] In brief, four carbons are lumped into a single CG bead, where σ and ε values are 4.3 Å and 2.625 kJ mol^{-1} for the SWNT−SWNT interaction, and 4.7 Å and 2.7 kJ mol^{-1} for the SWNT−lipid tail interaction. Beads of the CG SWNT are connected by a weak harmonic potential $V_{bond}(R)$ with an equilibrium distance R_{bond} = 2.84 Å ($V_{bond}(R) = (1/2)K_b\{R - R_{bond}\}^2$, where K_b = 20 000 kJ mol^{-1} nm^{-2}) and a weak harmonic angle potential with an equilibrium angle θ_0 = 120° ($V_{angle}(\theta) = (1/2)K_\theta\{\cos(\theta) - \cos(\theta_0)\}^2$, where K_θ = 1500 kJ mol^{-1}), leading to a rigid rod rather than a flexible tube. This rigid SWNT is reasonably considered in this work, since the length of the simulated SWNT is much shorter than the persistence length of SWNT. Note that Monticelli recently parametrized the CG fullerene with the "SC4" bead,[51] where σ and ε values for the fullerene−fullerene interaction are same as those for the SWNT−SWNT interaction in this work. The interaction strength between SWNT and lipid tails are assigned within the framework of the MARTINI FF, but our previous simulations showed that the weaker SWNT−lipid tail interaction is required to predict the experimentally observed structures of self-assembled SWNT−lipid complex,[19] which was also observed from simulations by the Sansom group.[38] Therefore, the reduced ε value for SWNT−lipid tail was used in this work, as described above.

The equilibrated self-assembled coordinates of the 20 nm long (18,0) SWNTs wrapped with lipids or PEGylated lipids were obtained from our previous work,[19] as shown in Figure 1

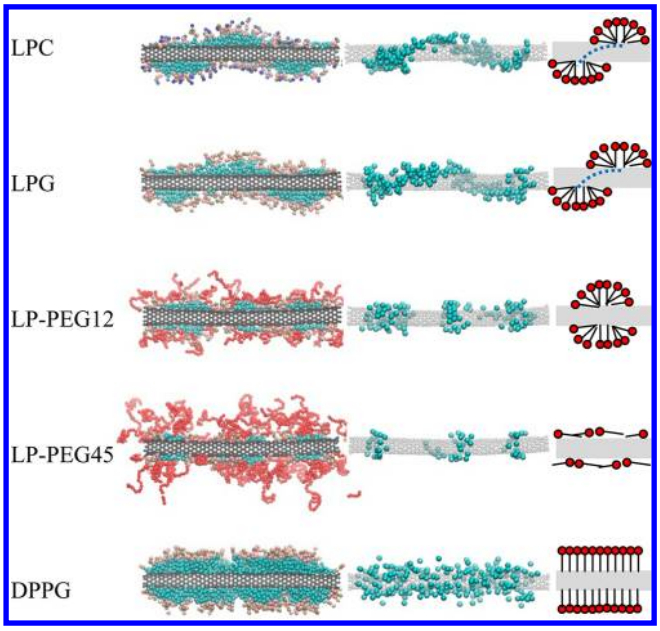

Figure 1. Final configurations of the self-assembled SWNT−lipid complex obtained from our previous simulations.[19] A cross section of the lipid−SWNT complex (left images), a whole section of the SWNT with the ending (the last carbon) CG beads of the lipid tail (middle images), and schematic illustrations (right images) are depicted. For the left and middle images, black, light blue, pink, brown, blue, and red beads, respectively, represent SWNT, lipid tail, glycerol, phosphate, choline, and PEG. The images were created with Visual Molecular Dynamics.[55]

and Table 1. Models for lipids, water, and ions were taken directly from the MARTINI lipid FF. A cutoff of 12 Å was used for the LJ potential and electrostatic interactions. The LJ and Coulomb potentials were smoothly shifted to zero between 9 and 12 Å, and between 0 and 12 Å, respectively. A temperature of 310 K and a pressure of 1 bar were maintained by applying a Berendsen thermostat in the NPT ensemble with semi-isotropic and isotropic pressure couplings for bilayer systems and other systems, respectively.[52] Simulations were performed for 500 ns with a time step of 20 fs (or 8 fs for PEGylated lipid systems, which is lower than the typical time step because of inclusion of PEG dihedral potentials) on computational facilities supported by the Supercomputing Center/Korea Institute of Science and Technology Information with supercomputing resources including technical support [KSC-2012-C2-53]. The last 100 ns was used for analyses.

Simulations of Three SWNT−Lipid Complexes in Water. Three copies of the equilibrated SWNT−lipid complex (pure SWNT, LPC, or LP-PEG12) were randomly positioned away from each other and solvated with ∼120 000 CG waters

Table 1. List of All Simulations

		SWNT–lipid complex					
		no. of complex	no. of lipids per complex	no. of charges	M_w of PEG	init conformation	no. of DPPC in bilayer
no bilayer	SWNT	3					
	LPC	3	182			helical wrapping	
	LP-PEG12	3	139	139	550	hemimicelle	
bilayer	SWNT	1					1152
	LPC	1	182			helical wrapping	1152
	LPG	1	196	196		helical wrapping	1152
	LP-PEG12	1	139	139	550	hemimicelle	1152
	LP-PEG45	1	76	76	2000	random adsorption	1152
	DPPG	1	254	254		cylindrical micelle	1152

(representing ~480 000 real waters) in a periodic box of size 25 nm/side. For LP-PEG12, 417 counterions (Na^+) were added to neutralize the system (Table 1 and Figure 2).

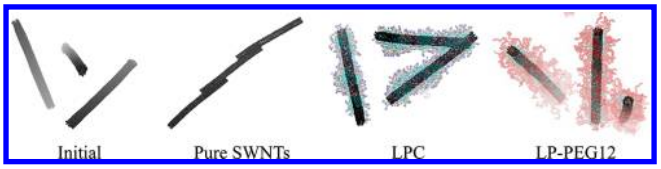

Figure 2. Snapshots at the beginning (0 ns, left) and end (500 ns, columns 2–4) of the simulations of three copies of the SWNT–lipid complex in water. Initial configuration is shown only for the system without lipids. For clarity, the lipid and PEG beads are transparent, and water and ions are omitted.

Simulations of a SWNT–Lipid Complex in DPPC Bilayer. A single SWNT–lipid complex was added to the equilibrated lipid bilayer system, which consists of 1152 dipalmitoylglycerophosphocholine (DPPC) lipids (576 DPPCs/leaflet). A SWNT–lipid complex was positioned above the lipid bilayer with a distance of 5 nm between the SWNT and bilayer centers. The final simulated system consists of one SWNT–lipid complex, 1152 DPPC lipids, ~35 000 CG waters (~140 000 real waters), and 0–254 counterions (Na^+) in a periodic box of size 19 × 19 × 18 nm^3 (Table 1).

RESULTS AND DISCUSSION

Configurations of 20 nm long SWNT–lipid complexes obtained from our previous work are shown in Figure 1.[19] These complexes are named "LPC", "LPG", "LP-PEG12", "LP-PEG45", and "DPPG", respectively, representing lysophosphatidylcholine, lysophosphatidylglycerol, PEGylated lysophospholipid with PEG M_w's of 550 and 2000, and dipalmitoylglycerophosphoglycerol. These complexes were visualized from our previous self-assembly simulations of mixtures of a SWNT and lipids, which showed that LPC and LPG formed the helical wrapping of a "half-cylinder" along the SWNT, while LP-PEG12 and LP-PEG45 showed "hemimicelle" or almost "random adsorption". DPPG showed the conformation of the "cylindrical micelle", indicating the effects of the lipid structure, favorably compared with experimental data. The simulated systems of these complexes in water and in lipid bilayers are listed in Table 1.

Effects of the SWNT–Lipid Structure on Interparticle Aggregation. Three copies of the SWNT–lipid complex were simulated in water to understand the effects of the complex structure on interparticle aggregation. Figure 2 shows the initial and final snapshots for simulations. For the system with pure SWNTs, all SWNTs aggregate, apparently because of strong hydrophobic interaction. For LPC, two SWNTs aggregate, while no aggregation is shown for LP-PEG12. Figure 3 shows

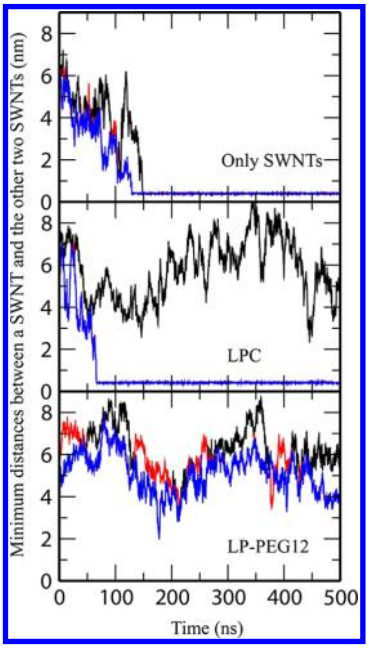

Figure 3. Minimum distances between one SWNT and the other two SWNTs as a function of time. Since each system includes three SWNTs, three minimum distances are shown with different colors.

minimum distances between one SWNT and the other two SWNTs as a function of the simulation time. For the system with pure SWNTs, all minimum distances reach the steady-state value of <0.5 nm at around 150 ns, again indicating interparticle aggregation. For LPC, one SWNT molecule does not aggregate with others, showing less aggregation, although it cannot be ruled out that aggregation might eventually occur in all SWNTs that do not show it for the short runs. LP-PEG12 shows no aggregation for the whole simulation time, indicating that PEG chains significantly inhibit aggregation. Figure 4 shows radial distribution functions (RDFs) of beads of two SWNTs with respect to the surface of the other SWNT. Pure SWNTs show the highest peak around 0.5 nm, while in LP-PEG12 the RDF value gradually increases after 4 nm. These indicate that pure SWNTs in water strongly tend to aggregate because of the hydrophobic interaction, but the modification of SWNTs with lipids and PEGylated lipids can reduce aggregation, as observed in experiment.[18] In particular, complete dispersion of LP-PEG12 agrees with the experiment

dx.doi.org/10.1021/jp308912r | J. Phys. Chem. B 2013, 117, 1337–1344

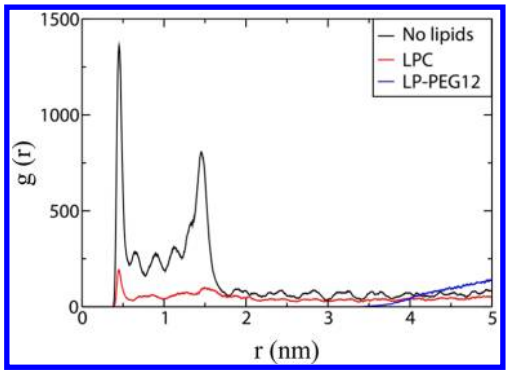

Figure 4. Radial distribution functions (RDFs) of beads of two SWNTs with respect to the surface of the other SWNT.

by Das et al., which showed that the SWNT modification with PEGylated lysophospholipids (PEG M_w = 550) caused excellent dispersing ability.[28]

To understand the effect of the surface modification of SWNTs on diffusivity, the diffusion coefficients (D) of SWNTs were calculated. The slopes of the mean-square displacements (MSD) of the center of mass (COM) of SWNT versus time were calculated (D_{PBC}) and corrected for finite size effects using the formula[53] $D = D_{PBC} + K_B T\xi/6\pi\eta L$, where K_B is Boltzmann's constant, L is the cubic box length, ξ = 2.837 297 (which has been found to be the coefficient for the correction factor for particles on a cubic lattice interacting electrostatically via Poisson's equation with Ewald summation), and viscosity η = 0.72 at 310 K for CG water.[54] In Table 2, the D value of the

Table 2. Diffusion Coefficients (D) of the SWNT−Lipid Complex

	no. of SWNTs in an aggregate	D (10^{-7} cm^2 s^{-1})
no lipids	3	6.34 ± 0.36
LPC	1	8.86 ± 0.65
	2	6.89 ± 0.96
LP-PEG12	1	5.74 ± 0.51
	1	6.29 ± 0.06
	1	6.19 ± 0.53

aggregated three SWNTs without lipids is lower than those of the aggregated two SWNTs and the other unaggregated SWNT in LPC. For LPC, diffusivity of the aggregated two SWNTs is slower than that of the other unaggregated one. These indicate that the aggregates with more molecules have slower diffusivities. Three unaggregated SWNTs of LP-PEG12 have almost the same diffusivities as does the aggregate of pure SWNTs, presumably because attachment of PEG significantly increases the particle size.

Effects of the SWNT−Lipid Structure and PEGylation on Insertion of SWNT into the Bilayer. To understand the effects of the self-assembled SWNT−lipid structure on their interactions with lipid bilayers, a single SWNT−lipid complex was simulated with DPPC bilayer, as listed in Table 1. Figure 5 shows snapshots of simulations of the SWNT−lipid complex interacting with lipid bilayers. Pure SWNT without lipids, which is initially positioned close to the bilayer, binds to the upper leaflet of the bilayer at the beginning of the simulation and induces membrane curvature, presumably because of hydrophobic interaction between SWNT and lipid tails in the bilayer. Then, the SWNT inserts into the hydrophobic region of the bilayer, which completely ends by 50 ns. LPC, LPG, and LP-PEG12 also show the insertion of SWNTs, but those SWNT−lipid complexes more slowly insert into the bilayer. The configurations of the inserted SWNTs and lipid bilayers do not change much after 200 ns. In Figure 6, energies for each system were calculated, showing that the energies reach steady-state values within 200 ns, indicating that the SWNT−bilayer systems are equilibrated within the simulated time scales. These results indicate that the hydrophobic interaction between SWNT and bilayer induces the SWNT insertion, and the extent of insertion can be reduced by lipids and PEGs wrapping on SWNTs. In particular, the SWNT−lipid complexes induce the higher extent of membrane curvature, where the complexes insert into the positively curved region of the bilayer. For LP-PEG45 and DPPG, SWNTs do not insert into the bilayer.

Mass densities of the SWNT−lipid complex and the bilayer lipids are plotted in Figure 7. LPC, LPG, and LP-PEG12 show the SWNT−lipid mass in the bilayer region, whereas LP-PEG45 and DPPG do not show any SWNT−lipid mass in the bilayer region, indicating no penetration of the complex into the bilayer, consistent with observations in Figure 5. In LPC, LPG, and LP-PEG12, headgroups and tails of lipids wrapping on SWNTs overlap mostly with those of the bilayer lipids, indicating the complete adsorption of the wrapping lipids into the bilayer. In DPPG, the complex binds to the bilayer surface, apparently because of the electrostatic interactions between lipid headgroups of the SWNT complex and the bilayer, while LP-PEG45 does not even show the binding, indicating the effect of long PEG chains.

The structure of the SWNT−lipid complex modulates the extent of the binding and insertion of SWNTs into the bilayer, as observed above. To investigate the atomic-scale details of the complex structure, RDFs of lipid beads of the SWNT−lipid complex with respect to the SWNT surface were calculated. In Figure 8, profiles for the hydrocarbon-tail beads show the highest peaks at ∼0.5 nm for all systems, indicating that SWNTs are wrapped mostly by hydrocarbon tails because of their hydrophobic interactions. The lipid-headgroup beads in LPC, LP-PEG12, and LP-PEG45 are broadly distributed over the range 0.5−2.5 nm, with those more concentrated at around 0.5−1.5 nm, while those in DPPG are much more concentrated around 1.5−2.5 nm. Note that the SWNT−DPPG complex forms the cylindrical-micelle shape, where lipids are mostly perpendicular with respect to the SWNT surface (Figure 1). This can be confirmed by the density profiles for DPPG that show the thick layer of hydrocarbon tails and much more concentrated headgroups around 1.5−2.5 nm. These results imply that since the cylindrical-micelle conformation has less extent of the lipid-layer curvature, the SWNT can be wrapped more tightly by charged headgroups, which can weaken the hydrophobic interactions between SWNTs and bilayer tails. For LP-PEG45, although the SWNT is wrapped by fewer charged headgroups, SWNT does not insert into the bilayer because of the thick layer of long hydrophilic PEG chains on the SWNT surface, which can also weaken the hydrophobic interaction between the SWNT and bilayer tail.

These results indicate that the binding and insertion of SWNTs into the bilayer can be significantly modulated by the self-assembled structure of the SWNT−lipid complex and the length of PEG. The SWNT−lipid complexes with the shape of helical wrapping and hemimicelle insert into the bilayer because of hydrophobic interaction between SWNTs and lipid tails of the bilayer, while the complexes with other shapes do not. The

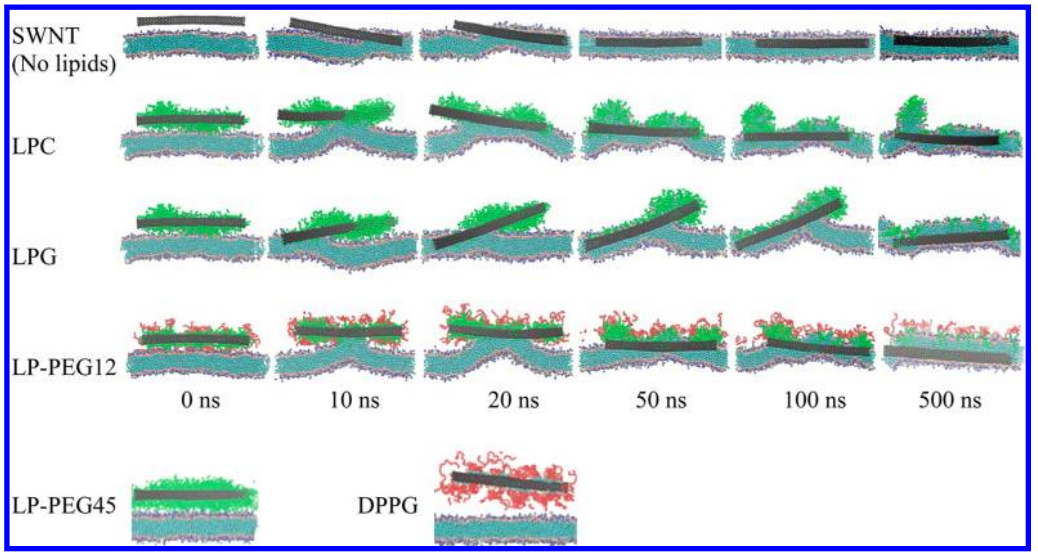

Figure 5. Snapshots of the simulations of the SWNT−lipid complex inserted into lipid bilayers (SWNT, LPC, LPG, and LP-PEG12), as functions of time. For LP-PEG45 and DPPG, only final configurations are shown, since no insertion was observed for the whole simulation time. To distinguish from the bilayer lipids, the SWNT-wrapping lipids are colored in green. For clarity, water and ions are omitted.

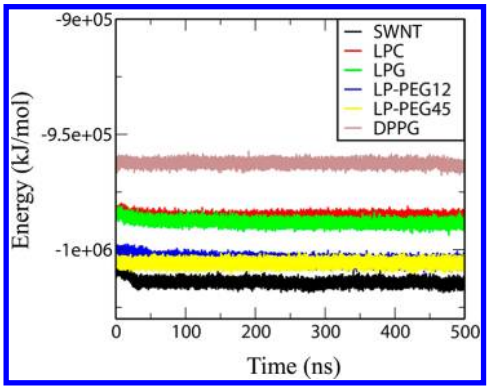

Figure 6. Energies of simulation systems as a function of time.

tight wrapping of the charged lipid headgroups on SWNTs can weaken the hydrophobic interaction, leading to the reduced extent of the SWNT penetration, although the electrostatic interaction helps the complex bind to the bilayer surface. Besides the electrostatic effect, relatively long hydrophilic PEG chains (M_w = 2000) also inhibit the insertion of SWNT into the bilayer. The SWNT−lipid complexes with the shape of helical wrapping and hemimicelle insert into the bilayer, while the complexes with other shapes do not. Note that the radius of the simulated SWNT is ∼1.4 nm, and the SWNT length is only 20 nm, which is much shorter than those in experiments. It cannot be ruled out that the thickness of SWNTs and different orientations of longer SWNTs on lipid bilayers may influence the binding and insertion of SWNTs.

Membrane Disorder and Curvature Induced by the SWNT−Lipid Complex. Figure 9 shows the numbers of hydrocarbon-tail beads of SWNT-wrapping lipids and the bilayer lipids within a distance of 0.6 nm from the SWNT surface. In LPC, LPG, and LP-PEG12, the numbers of the SWNT-wrapping lipids decrease, while the numbers of the bilayer lipids increase. This indicates that when the SWNT−lipid complexes insert into the bilayer, the SWNT-wrapping lipids are randomly mixed with the bilayer lipids; thus the SWNT interacts mostly with the bilayer lipids. The lipid numbers reach apparent steady-state values at ∼300 ns,

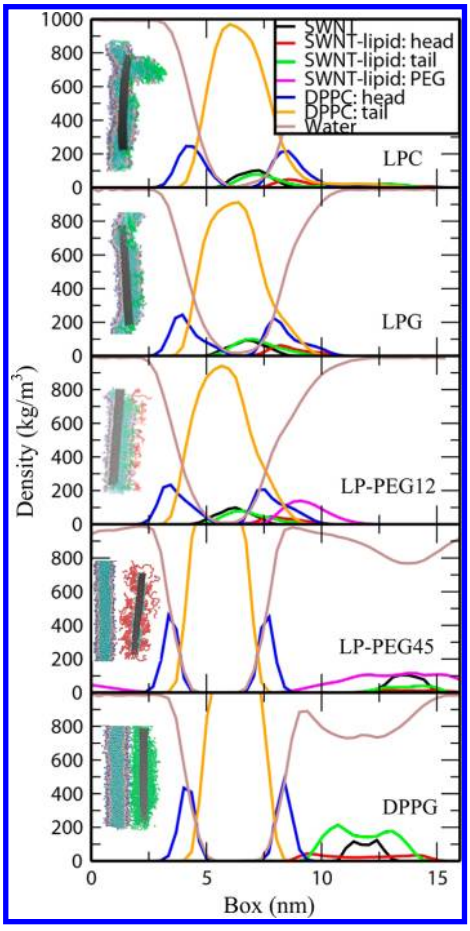

Figure 7. Mass density profiles of the SWNT−lipid complex and DPPC bilayer.

indicating that the insertion process is complete by 300 ns. For LP-PEG45, the number of the bilayer lipids equals zero for the whole simulation time, again confirming that the SWNT with long PEG chains does not insert into the bilayer.

dx.doi.org/10.1021/jp308912r | J. Phys. Chem. B 2013, 117, 1337−1344

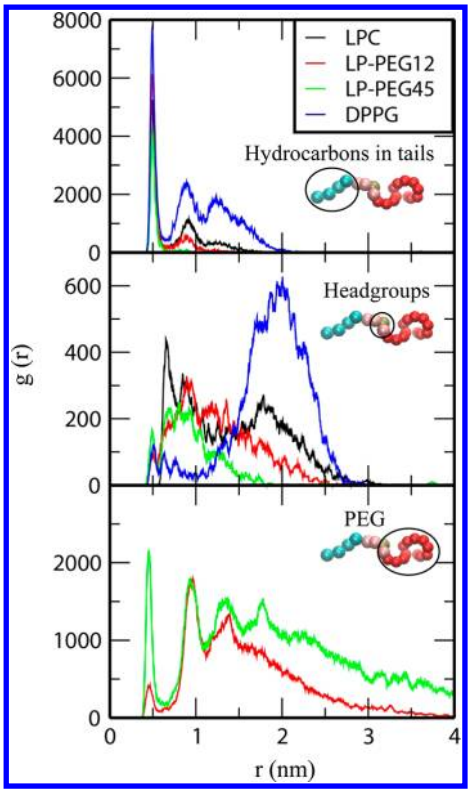

Figure 8. RDFs of lipid beads of the SWNT−lipid complex with respect to the surface of the SWNT.

Insertion of SWNTs and lipids into the bilayer may disorder lipids in the bilayer. To investigate this, the DPPC tail conformational order was quantified by the order parameter $S_{CC} = (3/2)\langle\cos^2 \theta_z\rangle - 1/2$, where θ_z is the angle that the vector connecting carbons C_{n-1} to C_{n+1} makes with the z-axis. The bracket indicates averaging over time and over all molecules in the simulation. Order parameters can vary between 1 (perfect orientation in the interface normal direction) and −1/2 (perfect orientation perpendicular to the normal). Figure 10 shows that the inserted SWNTs disorder DPPC tails in the bilayer. The order-parameter values for LPC, LPG, and LP-PEG12 do not significantly differ, indicating that different types of lipids do not significantly influence the extent of disorder.

This SWNT-induced disorder may be relevant to the bilayer curvature observed in Figure 5. The SWNT-induced positive curvature is visualized in Figure 11. The inserted SWNT is positioned at the lower leaflet of the bilayer, where the entire four tail beads of the neighboring lipids contact the SWNT surface. The top region of the SWNT surface interacts mainly with the ending tail beads (C4) of the upper leaflet. This visualized structure is rationalized by calculating the RDFs between lipid tails and SWNT beads. The RDF values for C1, C2, and C3 are very close at ∼0.5 nm, indicating that all tail beads of the neighboring lipids evenly wrap the SWNT surface. The value for C4 is higher than others, indicating that some portions of the SWNT interact only with the ending tail beads of lipids. These results support that the inserted SWNT is wrapped by the entire tails of lipids in the lower leaflet, as well as by the ending carbons of the tail in the upper leaflet, which induces bilayer disorder and positive curvature. These indicate that the membrane penetration and curvature can be modulated by the SWNT−lipid complex and the PEG length.

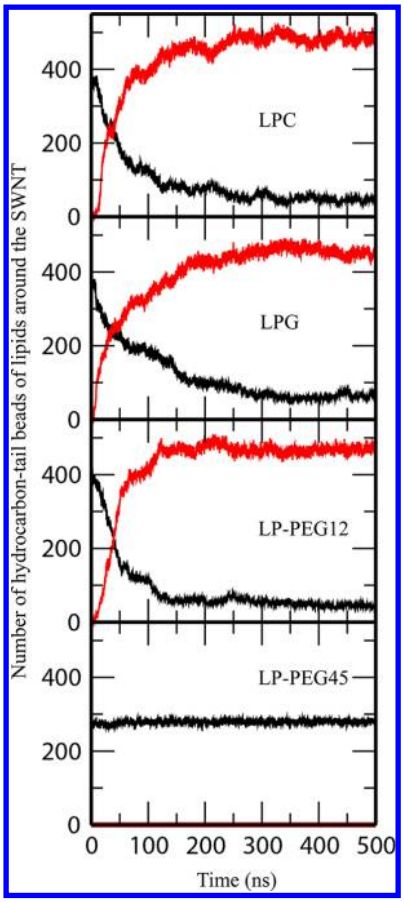

Figure 9. Number of hydrocarbon-tail beads of the SWNT-wrapping lipids (black lines) and the bilayer lipids (red lines) within a distance of 0.6 nm from the SWNT surface, as a function of time.

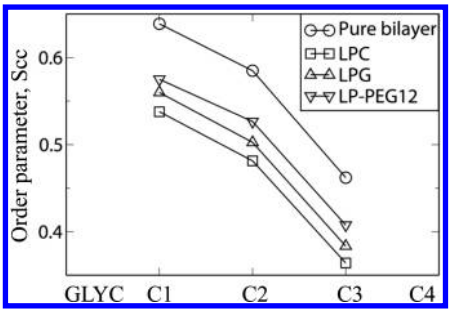

Figure 10. Order parameters of DPPC tails in bilayers. GLYC designates the bead for glycerol in DPPC, and C1−C4 are beads for the tail.

■ CONCLUSIONS

SWNTs wrapped with different types of lipids and PEGylated lipids were simulated with lipid bilayers using the MARTINI coarse-grained (CG) force field (FF). The CG SWNT and PEG were previously parametrized by our group, which successfully predicted the self-assembled structure of the SWNT−lipid complex and the phase behavior of mixtures of lipids and PEGylated lipids. We first simulated three copies of pure SWNTs and the wrapped SWNTs in water, showing that all pure SWNTs aggregate, lipid-wrapped SWNTs partially aggregate, but PEGylated lipid-wrapped SWNTs completely disperse, indicating that the wrapping of lipids and PEGylated lipids reduces the extent of interparticle aggregation. In

dx.doi.org/10.1021/jp308912r | J. Phys. Chem. B 2013, 117, 1337−1344

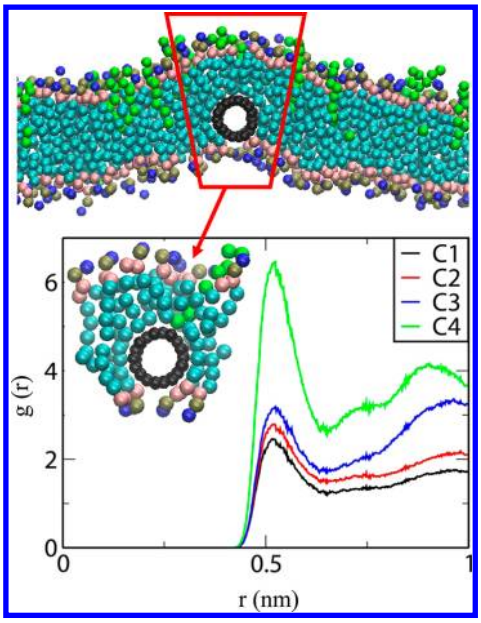

Figure 11. Snapshot at the end of the LPG simulation with respect to the cross section of SWNT (top), and RDFs between the lipid tail (C1−C4) and SWNT beads.

particular, complete dispersion induced by short PEG chains (M_w = 550) agrees with experiment.

Simulations of a single SWNT or SWNT−lipid complex with lipid bilayers showed that pure SWNTs, and SWNTs wrapped with lysophospholipids and short PEG chains, which have conformations of "helical half-cylinder" and "hemimicelle", penetrate into the hydrophobic tail region of the bilayer, while those wrapped with phospholipids and long PEG chains, which have conformations of "cylindrical micelle" and "random adsorption", do not. These results indicate that the hydrophobic interactions between SWNTs and the bilayer tails induce the SWNT insertion into the bilayer, but this can be inhibited by the tight wrapping of charged lipid headgroups and long hydrophilic PEG chains, although the electrostatics between charged headgroups helps the SWNT complex bind to the bilayer surface. The inserted SWNT beads are surrounded by entire tails of neighboring lipids in one leaflet of the bilayer, which induces positive curvature along the SWNT. These results indicate that the SWNT−lipid structure and the PEG length can significantly influence interparticle aggregation, the insertion of SWNT into the bilayer, and membrane curvature.

AUTHOR INFORMATION

Corresponding Author

*E-mail: leeh@dankook.ac.kr.

Notes

The authors declare no competing financial interest.

REFERENCES

(1) Bianco, A.; Kostarelos, K.; Prato, M. *Curr. Opin. Chem. Biol.* **2005**, *9*, 674−679.
(2) Lacerda, L.; Bianco, A.; Prato, M.; Kostarelos, K. *Adv. Drug Delivery Rev.* **2006**, *58*, 1460−1470.
(3) Lacerda, L.; Raffa, S.; Prato, M.; Bianco, A.; Kostarelos, K. *Nano Today* **2007**, *2*, 38−43.
(4) Kam, N. W. S.; Jessop, T. C.; Wender, P. A.; Dai, H. *J. Am. Chem. Soc.* **2004**, *126*, 6850−6851.
(5) Kam, N. W. S.; O'Connell, M.; Wisdom, J. A.; Dai, H. *Proc. Natl. Acad. Sci. U.S.A.* **2005**, *102*, 11600−11605.
(6) Liu, Z.; Cai, W.; He, L.; Nakayama, N.; Chen, K.; Sun, X.; Chen, X.; Dai, H. *Nat. Nanotechnol.* **2007**, *2*, 47−52.
(7) Hirsch, A.; Vostrowsky, O. *Top. Curr. Chem.* **2005**, *245*, 193−237.
(8) Liu, Z.; Robinson, J. T.; Tabakman, S. M.; Yang, K.; Dai, H. *Mater. Today* **2011**, *14*, 316−323.
(9) Kuzmany, H.; Kukovecz, A.; Simon, F.; Holzweber, M.; Kramberger, C.; Pichler, T. *Synth. Met.* **2004**, *141*, 113−122.
(10) Karousis, N.; Tagmatarchis, N.; Tasis, D. *Chem. Rev.* **2010**, *110*, 5366−5397.
(11) Ke, P. C.; Lamm, M. H. *Phys. Chem. Chem. Phys.* **2011**, *13*, 7273−7283.
(12) Richard, C.; Balavoine, F.; Schultz, P.; Ebbesen, T. W.; Mioskowski, C. *Science* **2003**, *300*, 775−778.
(13) Yurekli, K.; Mitchell, C. A.; Krishnamoorti, R. *J. Am. Chem. Soc.* **2004**, *126*, 9902−9903.
(14) Matarredona, O.; Rhoads, H.; Li, Z.; Harwell, J. H.; Balzano, L.; Resasco, D. E. *J. Phys. Chem. B* **2003**, *107*, 13357−13367.
(15) Qiao, R.; Ke, P. C. *J. Am. Chem. Soc.* **2006**, *128*, 13656−13657.
(16) O'Connell, M. J.; Bachilo, S. H.; Huffman, C. B.; Moore, V. C.; Strano, M. S.; Haroz, E. H.; Rialon, K. L.; Boul, P. J.; Noon, W. H.; Kittrell, C.; et al. *Science* **2002**, *297*, 593−596.
(17) Kam, N. W. S.; Liu, Z.; Dai, H. *J. Am. Chem. Soc.* **2005**, *127*, 12492−12493.
(18) Wu, Y.; Hudson, J. S.; Lu, Q.; Moore, J. M.; Mount, A. S.; Rao, A. M.; Alexov, E.; Ke, P. C. *J. Phys. Chem. B* **2006**, *110*, 2475−2478.
(19) Lee, H.; Kim, H. *J. Phys. Chem. C* **2012**, *116*, 9327−9333.
(20) Lin, S.; Keskar, G.; Wu, Y.; Wang, X.; Mount, A. S.; Klaine, S. J.; Moore, J. M.; Rao, A. M.; Ke, P. C. *Appl. Phys. Lett.* **2006**, *89*, 143118.
(21) Lu, Q.; Moore, J. M.; Huang, G.; Mount, A. S.; Rao, A. M.; Larcom, L. L.; Ke, P. C. *Nano Lett.* **2004**, *4*, 2473−2477.
(22) Liu, Z.; Sun, X.; Nakayama-Ratchford, N.; Dai, H. *ACS Nano* **2007**, *1*, 50−56.
(23) Liu, Z.; Winters, M.; Holodniy, M.; Dai, H. *Angew. Chem., Int. Ed.* **2007**, *46*, 2023−2027.
(24) Liu, Z.; Chen, K.; Davis, C.; Sherlock, S.; Cao, Q.; Chen, X.; Dai, H. *Cancer Res.* **2008**, *68*, 6652−6660.
(25) Liu, Z.; Davis, C.; Cai, W.; He, L.; Chen, X.; Dai, H. *Proc. Natl. Acad. Sci. U.S.A.* **2008**, *105*, 1410−1415.
(26) Liu, Z.; Robinson, J. T.; Sun, X.; Dai, H. *J. Am. Chem. Soc.* **2008**, *130*, 10876−10877.
(27) Welsher, K.; Liu, Z.; Daranciang, D.; Dai, H. *Nano Lett.* **2008**, *8*, 586−590.
(28) Brahmachari, S.; Das, D.; Shome, A.; Das, P. K. *Angew. Chem., Int. Ed.* **2011**, *50*, 11243−11247.
(29) Liu, X.; Tao, H.; Yang, K.; Zhang, S.; Lee, S. T.; Liu, Z. *Biomaterials* **2011**, *32*, 144−151.
(30) Lopez, C. F.; Nielsen, S. O.; Moore, P. B.; Klein, M. L. *Proc. Natl. Acad. Sci. U.S.A.* **2004**, *101*, 4431−4434.
(31) Nielsen, S. O.; Ensing, B.; Ortiz, V.; Moore, P. B.; Klein, M. L. *Biophys. J.* **2005**, *88*, 3822−3828.
(32) Lopez, C. F.; Nielsen, S. O.; Ensing, B.; Moore, P. B.; Klein, M. L. *Biophys. J.* **2005**, *88*, 3083−3094.
(33) Hofinger, S.; Melle-Franco, M.; Gallo, T.; Cantelli, A.; Calvaresi, M.; Gomes, J. A. N. F.; Zerbetto, F. *Biomaterials* **2011**, *32*, 7079−7085.
(34) Makarucha, A. J.; Todorova, N.; Yarovsky, I. *Eur. Biophys. J.* **2011**, *40*, 103−115.
(35) Monticelli, L.; Salonen, E.; Ke, P. C.; Vattulainen, I. *Soft Matter* **2009**, *5*, 4433−4445.
(36) Shi, X.; Kong, Y.; Gao, H. *Acta Mech. Sin.* **2008**, *24*, 161−169.
(37) Shi, X.; Von Dem Bussche, A.; Hurt, R. H.; Kane, A. B.; Gao, H. *Nat. Nanotechnol.* **2011**, *6*, 714−719.
(38) Wallace, E. J.; Sansom, M. S. P. *Nano Lett.* **2008**, *8*, 2751−2756.
(39) Yang, K.; Ma, Y. Q. *Nat. Nanotechnol.* **2010**, *5*, 579−583.
(40) Skandani, A. A.; Zeineldin, R.; Al-Haik, M. *Langmuir* **2012**, *28*, 7872−7879.
(41) Pogodin, S.; Baulin, V. A. *ACS Nano* **2010**, *4*, 5293−5300.

(42) Kraszewski, S.; Bianco, A.; Tarek, M.; Ramseyer, C. *PLoS ONE* **2012**, *7*, e40703.
(43) Hess, B.; Kutzner, C.; van der Spoel, D.; Lindahl, E. *J. Chem. Theory Comput.* **2008**, *4*, 435−447.
(44) Lindahl, E.; Hess, B.; van der Spoel, D. *J. Mol. Model.* **2001**, *7*, 306−317.
(45) Van Der Spoel, D.; Lindahl, E.; Hess, B.; Groenhof, G.; Mark, A. E.; Berendsen, H. J. C. *J. Comput. Chem.* **2005**, *26*, 1701−1718.
(46) Marrink, S. J.; de Vries, A. H.; Mark, A. E. *J. Phys. Chem. B* **2004**, *108*, 750−760.
(47) Marrink, S. J.; Risselada, H. J.; Yefimov, S.; Tieleman, D. P.; de Vries, A. H. *J. Phys. Chem. B* **2007**, *111*, 7812−7824.
(48) Lee, H.; de Vries, A. H.; Marrink, S. J.; Pastor, R. W. *J. Phys. Chem. B* **2009**, *113*, 13186−13194.
(49) Lee, H.; Venable, R. M.; MacKerell, A. D.; Pastor, R. W. *Biophys. J.* **2008**, *95*, 1590−1599.
(50) Lee, H.; Pastor, R. W. *J. Phys. Chem. B* **2011**, *115*, 7830−7837.
(51) Monticelli, L. *J. Chem. Theory Comput.* **2012**, *8*, 1370−1378.
(52) Berendsen, H. J. C.; Postma, J. P. M.; van Gunsteren, W. F.; DiNola, A.; Haak, J. R. *J. Chem. Phys.* **1984**, *81*, 3684−3690.
(53) Yeh, I. C.; Hummer, G. *J. Phys. Chem. B* **2004**, *108*, 15873−15879.
(54) Fuhrmans, M.; Sanders, B. P.; Marrink, S. J.; de Vries, A. H. *Theor. Chem. Acc.* **2009**, *125*, 335−344.
(55) Humphrey, W.; Dalke, A.; Schulten, K. *J. Mol. Graphics* **1996**, *14*, 33−38.